INSTITUTE OF PHYSICS PUBLISHING JOURNAL OF MICROMECHANICS AND MICROENGINEERING

J. Micromech. Microeng. **15** (2005) S22–S29 doi:10.1088/0960-1317/15/7/004

A high-performance accelerometer with a fifth-order sigma–delta modulator

Yufeng Dong, Michael Kraft, Carsten Gollasch and William Redman-White

School of Electronics and Computer Science, University of Southampton, Highfield, Southampton, SO17 1BJ, UK

E-mail: yd02r@ecs.soton.ac.uk

Received 26 November 2004, in final form 6 March 2005
Published 20 June 2005
Online at stacks.iop.org/JMM/15/S22

Abstract

To verify the effectiveness of a higher order electromechanical sigma–delta modulator ($\Sigma\Delta$M), a micromachined accelerometer is fabricated. The in-plane sensor with fully differential structure has a mechanical noise floor below 1 μg Hz$^{-1/2}$, static sensitivity 16 pF g^{-1} and resonant frequency 325 Hz. FEM analyses are performed to verify these key parameters. The silicon-on-glass sensor is fabricated by deep reactive ion etching (DRIE) and anodic bonding. Compared with a second-order electromechanical $\Sigma\Delta$M, which only uses the sensing element as a loop filter, here it is cascaded with additional electronic integrators to form a fifth-order electromechanical $\Sigma\Delta$M, which leads to better signal to quantization noise ratio (SQNR). This novel approach is analysed and system level simulations are presented. A printed circuit board (PCB) prototype of this high-order $\Sigma\Delta$M loop was built and tested. The experimental data agree well with the simulation results.

(Some figures in this article are in colour only in the electronic version)

1. Introduction

High-performance micromachined inertial sensors with microgram resolution usually take advantage of closed loop control to increase their dynamic range, linearity and bandwidth. To avoid the electrostatic pull-in problems of purely analog force feedback control systems [1], sigma–delta modulator ($\Sigma\Delta$M) force feedback control schemes have become very attractive. Its output is digital in the form of a pulse density-modulated bitstream. Previous work has mainly focused on using a sensing element as a loop filter to form a second-order electromechanical $\Sigma\Delta$M [2, 3]. However, the equivalent dc gain of the mechanical integrator is relatively low and this leads to a much lower signal to quantization noise ratio (SQNR) for an electromechanical $\Sigma\Delta$M compared with an electronic, second-order $\Sigma\Delta$M analog to digital converter (ADC). It is desirable for high-performance inertial sensors to have a quantization noise level at least one order below both the mechanical noise and electronic noise level. Although SQNR can be improved by increasing the sampling frequency, this leads to an increase of the specification requirements for the interface circuitry and also to higher circuit noise [4]. Recently, higher order electromechanical $\Sigma\Delta$Ms, which employ additional electronic filters, have been designed [4, 5]. However, to verify the effectiveness of higher order electromechanical $\Sigma\Delta$Ms, a high-performance micromachined inertial sensor is required with both low mechanical and electronic noise. Bulk micromachining is preferred due to a large proof mass and low stress [6]. The design and fabrication of such an accelerometer is described in the following. Simulation and measurement results are presented incorporating the sensing element in a fifth-order $\Sigma\Delta$M, and are compared to conventional second-order electromechanical $\Sigma\Delta$Ms.

2. Sensor design

A lateral single-axis accelerometer is designed with a fully differential structure. Figure 1 shows a schematic diagram of the fully differential sensing element. The fully differential accelerometer has two sets of capacitors (Ca1 and Cb1, Ca2 and Cb2) connected in series. The capacitors Ca1 and Cb1

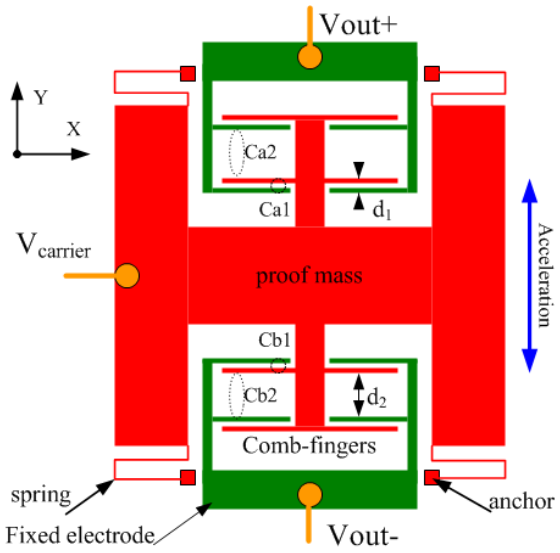

Figure 1. Schematic diagram of an accelerometer with a fully differential structure.

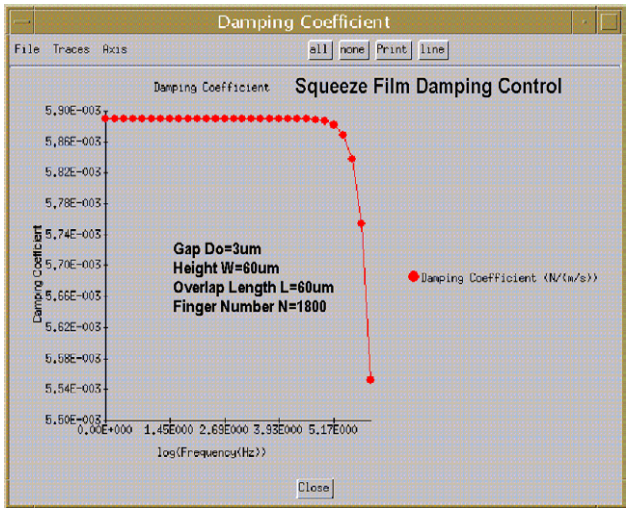

Figure 2. Squeeze-film damping simulated using CoventorWare™ (MemDamping Solver).

have a nominal gap of $d_1 = 3$ μm while Ca2 and Cb2 have a gap of $d_2 = 30$ μm. An excitation voltage is applied to the common electrode—the proof mass, while the fixed electrodes are connected to two pick-off amplifiers. The electrostatic force caused by the excitation voltage acts on the proof mass in symmetrically balanced directions and thus its effect is negligible. A large number of comb fingers (1800) are used as sensing capacitors with short and rigid finger electrodes, which results in very high resonant modes, well above any frequency of the feedback signal that potentially could excite the sense fingers and thus degrade the SQNR [1].

For micro-accelerometers, squeeze-film damping is an important effect for the dynamic behaviour; it occurs when the gap between two closely spaced parallel surfaces changes [7]. In figure 2(*a*), simulation using CoventorWare™ [8] (version 2001.3) with its solver MemDamping shows the damping coefficient of 1800 pair comb fingers (each 60 μm wide, overlap 60 μm) as a function of frequency of the proof mass motion. Using analytical expressions for the squeeze damping coefficient from [7] yields 5.9×10^{-3} N m^{-1} s^{-1}. This matches well with the simulation for low frequencies. The squeeze-film spring constant is negligible.

Table 1. Sensing element design parameters.

Mass of proof mass, m	1.2 mg
Spring constant, k	5 N m^{-1}
Damping coefficient, b	0.006 N m^{-1} s^{-1}
Resonant frequency	325 Hz
Quality factor	0.41
Cross axis sensitivity	−70 dB (Y–X) −77 dB (Y–Z)
Mechanical noise	0.85 μg Hz$^{-1/2}$
Static sensitivity	16.5 pF g^{-1}
Static sensing capacitance	21.03 pF
Sensing gap distance	3 μm
Thickness of proof mass	60 μm
Number of comb fingers	1800 (30 × 30 × 2)
Length of comb fingers	70 μm (overlap 60 μm)
Width of comb fingers	4 μm
Die area	4 × 4.8 mm^2

Modal analysis simulations using CoventorWare™ (version 2001.3) with its solver MemMech show that the resonant frequencies for the first mode along the y-axis is 323 Hz (see figure 3(*a*)), for the second mode along x-axis is 3.01 kHz (see figure 3(*b*)) and for the third mode along the z-axis is 3.96 kHz (see figure 3(*c*)), respectively. Analytical calculation for the first mode results in 325 Hz which is in good agreement with the simulation.

The sensor is nearly critically damped and has very low mechanical noise due to the large proof mass. Due to the large quantity of comb fingers, the sensor has a high static capacitance resulting in a high signal sensitivity and thus low electronic noise. Table 1 summarizes the design specifications of the sensing element.

3. Fabrication process

Fabricating the accelerometer using a silicon-on-glass process results in a low parasitic capacitance between the proof mass and the bottom nonconductive glass substrate. Furthermore, it is free of shear damping. By combining DRIE and anodic bonding, a large proof mass and very low stress can be achieved using single-crystalline bulk silicon. The fabrication process is illustrated in figure 4; it requires only three masks. The fabricated sensor is shown in figure 5(*a*), showing a part of the electrode area and in figure 5(*b*), showing a part of the spring structure.

4. Fifth-order electromechanical ΣΔM

4.1. Structure and performance

The diagram of a fifth-order electromechanical ΣΔM is shown in figure 6. $H_m(s)$ is the transfer function of the mechanical sensing element that converts the input inertial force signal into a displacement. It also is part of the loop filter. $H_{cp}(z)$ is the transfer function of a compensator for providing some phase lead to ensure the control loop stability, which is strongly

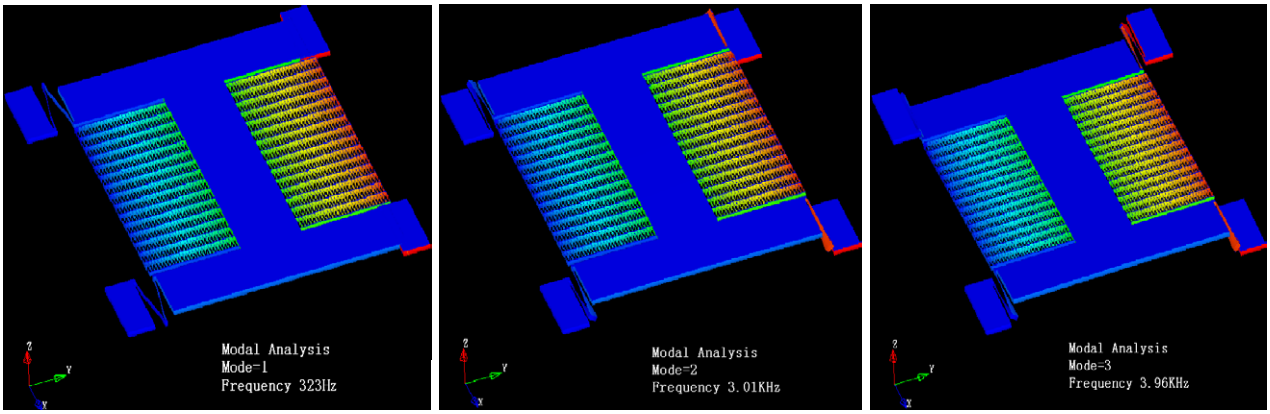

(*a*) (*b*) (*c*)

Figure 3. Modal analysis (*a*) mode 1, resonant frequency 323 Hz; (*b*) mode 2, resonant frequency 3.01 kHz; (*c*) mode 3, resonant frequency 3.96 kHz. Displacement is amplified by a factor of 100.

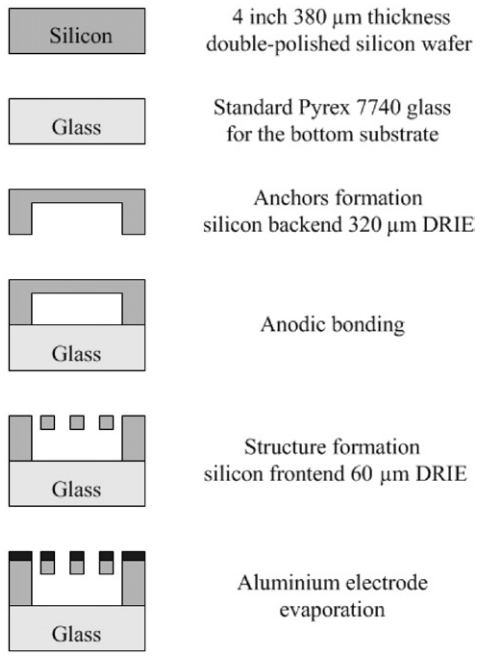

Figure 4. The fabrication process using bulk micromachining.

related to the damping coefficient of a sensing element. $H_e(z)$ is a third-order low-pass electronic filter and is implemented with distributed feedback topology. The electrical signal is then digitized by a one bit quantizer which is usually implemented by a clocked comparator. For linear system analysis, this can be modelled by a variable gain K_Q and added white quantization noise [9]. The signal pick-off is represented by two gain constants, K_{dc} and K_{cv}, which model the conversion from a proof mass deflection to a differential change in capacitance and from capacitance to a voltage, respectively. K_{fb} is the gain converting a feedback voltage V_{fb} to an electrostatic force on the proof mass. Due to the force feedback, closed loop, the displacement of the proof mass is very small, hence these transductions can be represented as constants. K_1 to K_3 are coefficients of the electronic integrators.

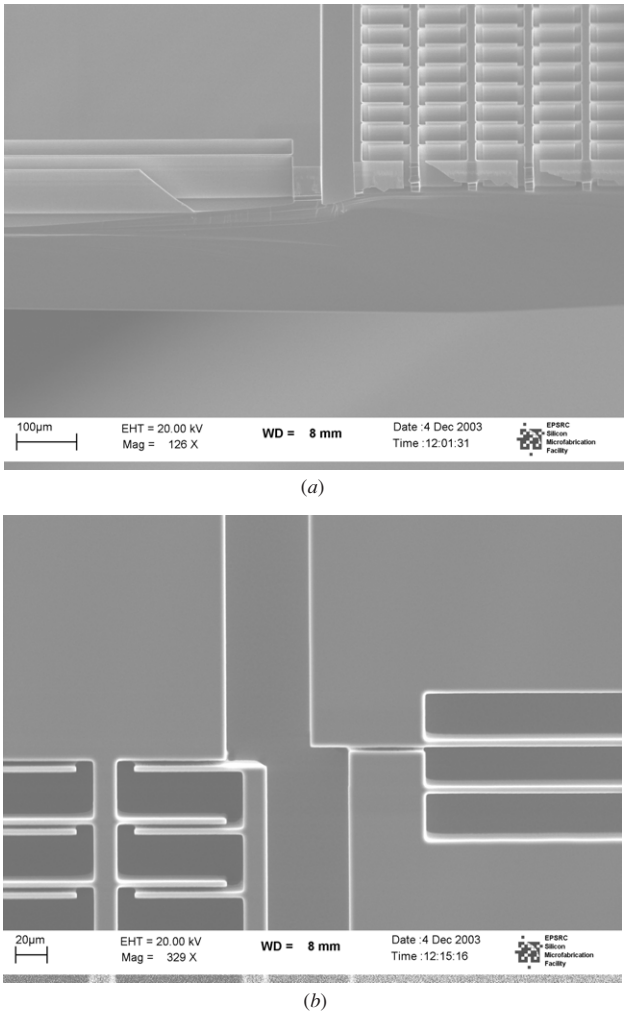

(*a*)

(*b*)

Figure 5. The SEM pictures of the fabricated sensor, showing (*a*) a part of the electrode area and (*b*) a part of the spring system.

With these assumptions standard linear control theory can now be applied to the system. The quantization noise transfer function (NTF) $Q_n(z)$ of the fifth-order electromechanical

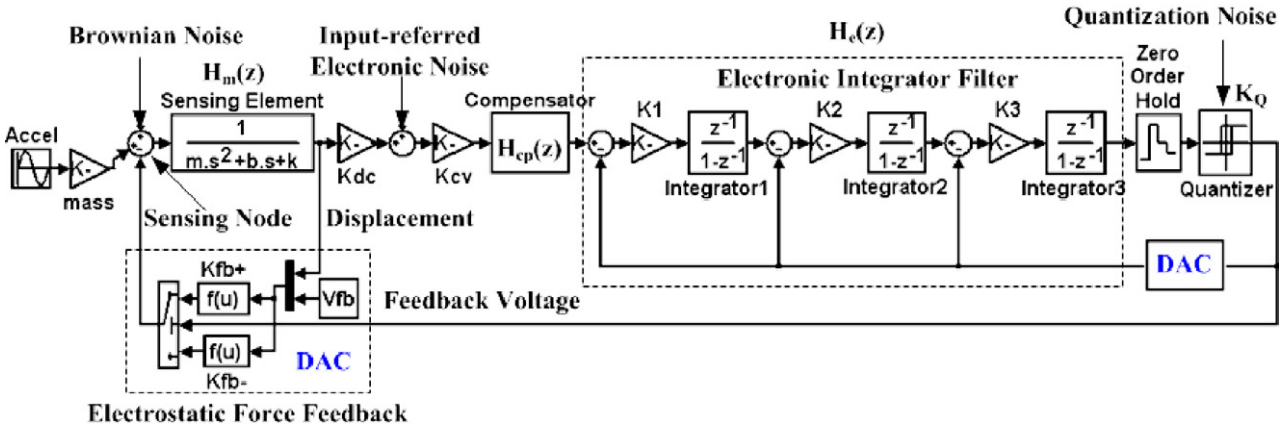

Figure 6. A fifth-order electromechanical ΣΔM.

ΣΔM shown in figure 6 can be derived as

$$Q_{\mathrm{n}}(z) = \frac{1}{1+K_{\mathrm{fb}}H_{\mathrm{m}}(z)K_{\mathrm{dc}}K_{\mathrm{cv}}K_{\mathrm{Q}}\prod_{i=1}^{3}K_i[I(z)]^3+\sum_{i=1}^{3}\prod_{j=i}^{3}K_jK_{\mathrm{Q}}[I(z)]^{4-i}} \tag{1}$$

where $I(z) = \frac{z^{-1}}{1-z^{-1}}$ is the transfer function (TF) of an electronic integrator and $H_{\mathrm{m}}(z)$ is the mechanical TF of a sensing element in discrete-time z-domain. This can be obtained by using an impulse-invariant transform [10]:

$$H_{\mathrm{m}}(z) = K_{\mathrm{m}}\frac{(1 - Zo_{\mathrm{m}} \cdot z^{-1}) \cdot z^{-1}}{(1 - p1_{\mathrm{m}} \cdot z^{-1}) \cdot (1 - p2_{\mathrm{m}} \cdot z^{-1})} \tag{2}$$

where K_{m}, Zo_{m}, $p1_{\mathrm{m}}$ and $p2_{\mathrm{m}}$ are the mechanical gain, zero and poles of a sensing element, respectively. Using the following approximations:

$$f \leqslant f_{\mathrm{b}} \ll f_{\mathrm{s}},$$

$$z^{-1} = \mathrm{e}^{-\mathrm{j}2\pi f/f_{\mathrm{s}}} = \cos\left(\frac{2\pi f}{f_{\mathrm{s}}}\right) - j\sin\left(\frac{2\pi f}{f_{\mathrm{s}}}\right) \approx 1 - \mathrm{j}\frac{2\pi f}{f_{\mathrm{s}}},$$

$$|1 - z^{-1}| \approx \left|\mathrm{j}\frac{2\pi f}{f_{\mathrm{s}}}\right| = \left|\mathrm{j}\pi\frac{f}{f_{\mathrm{b}}}\frac{2f_{\mathrm{b}}}{f_{\mathrm{s}}}\right| = \left|\mathrm{j}\pi\frac{f}{f_{\mathrm{b}}}\right| \cdot \left|\frac{1}{\mathrm{OSR}}\right| \ll 1, \tag{3}$$

where f_{b} is the signal bandwidth, f_{s} is the sampling frequency and OSR is the oversampling ratio given by $\mathrm{OSR} = \frac{2f_{\mathrm{s}}}{f_{\mathrm{b}}}$, the NTF can be simplified for low frequencies ($f \ll f_{\mathrm{s}}$) to

$$|Q_{\mathrm{n}}(z)|_{f\ll f_{\mathrm{s}}} \approx \frac{|1-z^{-1}|^5+|2-p1_{\mathrm{m}}-p2_{\mathrm{m}}||1-z^{-1}|^4+|(1-p1_{\mathrm{m}})(1-p2_{\mathrm{m}})||1-z^{-1}|^3}{K_{\mathrm{fb}}K_{\mathrm{dc}}K_{\mathrm{cv}}K_1K_2K_3K_{\mathrm{m}}(1-Zo_{\mathrm{m}})K_{\mathrm{Q}}+|(1-p1_{\mathrm{m}})(1-p2_{\mathrm{m}})|K_2K_3K_{\mathrm{Q}}}. \tag{4}$$

Equation (4) indicates that not only the order and topology of the electronic filters, but also the sensing element determines the quantization noise shaping in a high-order electromechanical ΣΔM. It can be seen from equation (4) that the noise shaping of the fifth-order electromechanical ΣΔM is strongly dependent on the position of the two poles $p1_{\mathrm{m}}$ and $p2_{\mathrm{m}}$, and thus has severe degradation compared with an electronic ΣΔM.

Figure 7 shows the simulated power spectral density of the output bitstreams of a second-order ΣΔM force feedback loop and the fifth-order ΣΔM loop, as shown in figure 6. The former only employs the sensing element as the loop filter (this approach has been reported by a number of researchers; see, e.g., [2, 3]). The input signal was assumed to be sinusoidal with a frequency of 128 Hz and an amplitude of 1 g. Both modulators were clocked at 2^{17} Hz, assuming 2^{10} Hz signal bandwidth this corresponds to an OSR of 64. As is obvious from figure 7, the noise floor has been reduced drastically; the SQNR has been improved by 60 dB.

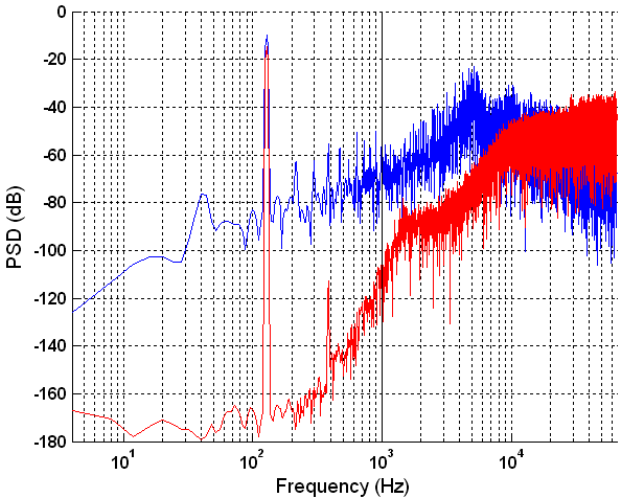

Figure 7. Noise shaping comparison between a second-order electromechanical ΣΔM and a fifth-order electromechanical ΣΔM.

4.2. Dead zone and limited cycles

For a second-order electromechanical ΣΔM, when the external input signal is zero, the digital feedback signal causes the proof mass to move up and down at one quarter of the sampling frequency f_{s}. The finite resonant frequency of the proof mass leads to a dead zone in which the output bitstream of the modulator does not change with variation of the input signal [11]. This dead zone can be greater than other noise sources in second order, electromechanical ΣΔMs, and thus it determines the minimum detectable acceleration. If the input amplitude is smaller than a minimal critical value, in

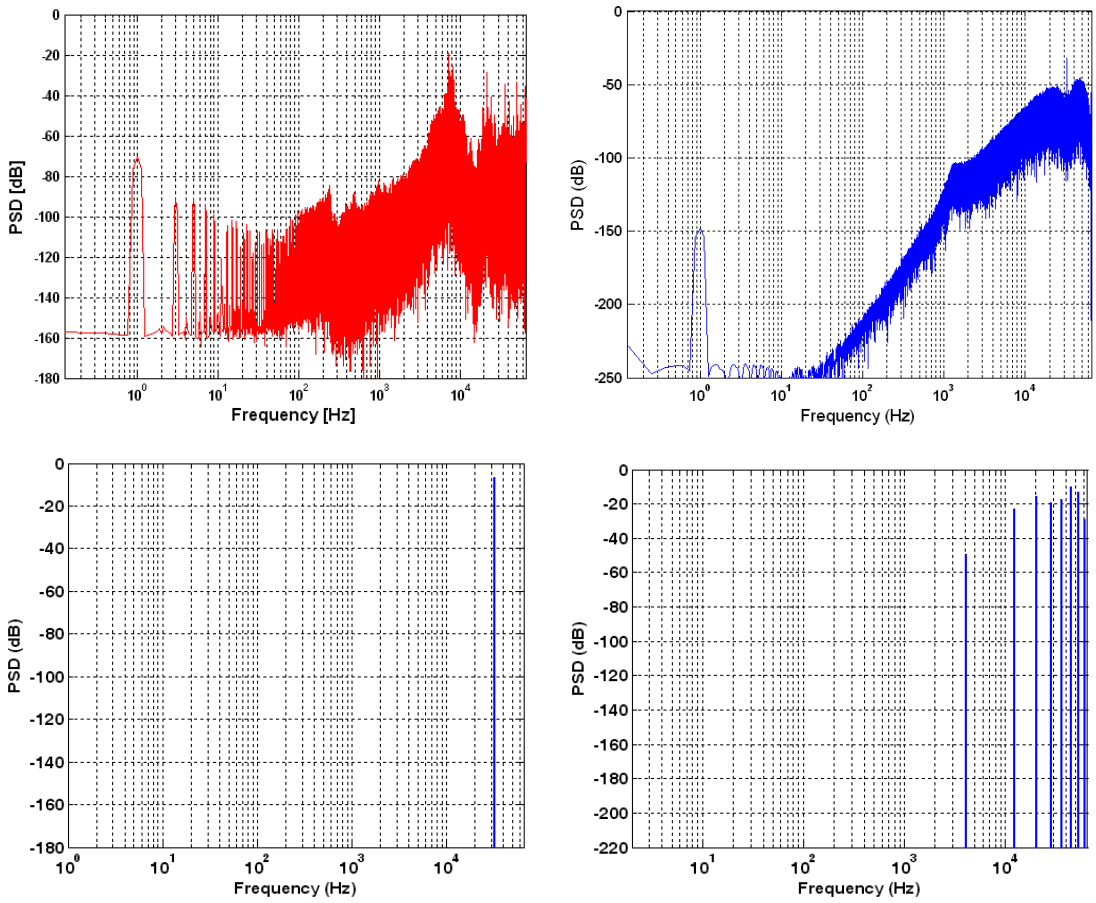

Figure 8. The power spectral density of the output bitstream assuming a full scale sensor dynamic range of ±1 g, OSR = 64 and 1024 Hz signal bandwidth: (*a*) a second-order ΣΔM force feedback loop with a sinusoidal input signal of 1 Hz and an amplitude of −54 dB in the top diagram. In the bottom diagram the amplitude was reduced to −60 dB: (*b*) a fifth-order ΣΔM force feedback loop with an input signal amplitude of −140 dB in the top figure and −160 dB in the bottom figure.

the spectrum of the output bitstream, there will be no visible peak at the input frequency, thus the modulator does not code the input signal any longer. Although increasing the sampling frequency can reduce the dead zone, this is at the sacrifice of increased circuit noise and higher power consumption. Figure 8(*a*) shows the power spectral density of the output bitstream in a second-order ΣΔM force feedback loop with a sinusoidal input signal of 1 Hz and an amplitude of 2×10^{-3} g (equivalent to −54 dB) in the top figure and an amplitude of 1×10^{-3} g (equivalent to −60 dB) in the bottom diagram. If the input amplitude drops below this critical amplitude of 2×10^{-3} g, the signal cannot be seen in the spectrum any longer, this is due to the dead zone of the control loop. In comparison, figure 8(*b*) shows the power spectral density of the output bitstream of the fifth-order ΣΔM force feedback loop with the same sinusoidal input signal but an amplitude of 1×10^{-7} g (equivalent to −140 dB). The signal still can be clearly seen in the top diagram, only reducing the amplitude further, it disappears due to the dead zone. The minimal critical amplitude for the fifth-order modulator is around −160 dB. The reduction of the dead zone in a higher order electromechanical ΣΔM is due to the additional electronic integrators in the forward path, which have greater gain at low frequencies. For most practical considerations the effect of a dead zone can be neglected.

Another effect of lower order ΣΔM loops is tonal behaviour. If the input signal of a ΣΔM is constant, the output signal easily exhibits a tonal behaviour due to limit cycles, and in some conditions these tones may be folded into the signal band, thus considerably reducing the SQNR [9, 12]. Low order ΣΔMs are particularly prone to exhibit such tonal behaviour. For simulation purposes, the constant input signal is approximated by a very low frequency signal (1 Hz). In the top figure 8(*a*), for the second-order electromechanical ΣΔM, such tones can be clearly identified in the spectrum as pronounced peaks in the signal band. As a consequence, the quantization noise cannot be considered as white any longer. In the fifth-order ΣΔM, the additional electronic integrators randomize the quantization error and thus whiten the quantization noise spectrum [12]. There is no evidence of limit cycles in the signal band of figure 8(*b*); therefore, limit cycles are greatly suppressed in the fifth-order electromechanical ΣΔM. In a hardware implementation, there inevitably additional noise source such as Brownian noise from the sensing element and electronic noise from the interface electronics, these act as a dither signal and further suppress the tonal behaviour due to limit cycles.

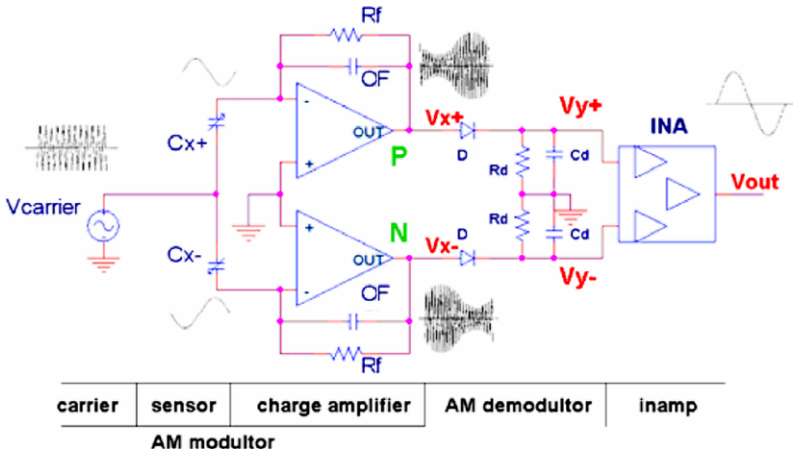

Figure 9. A fully differential capacitive interface using diode envelope demodulation.

4.3. Hardware implementation and measurement results

To verify the concept of a higher order electromechanical $\Sigma\Delta$M, a PCB prototype was implemented using surface mount commercial components. A continuous-time (CT) $\Sigma\Delta$M is preferred to a discrete-time (DT), switched capacitor (SC) $\Sigma\Delta$M for a PCB implementation; mainly because SC circuits require too many analog switches.

There are two separate digital to analog converters (DAC) in the high-order electromechanical $\Sigma\Delta$M (see figure 6). One DAC converts the feedback voltage to an electrostatic force on the proof mass, this is called the electromechanical DAC; the other DAC is to provide the electronic feedback signal to the electronic integrators. In CT $\Sigma\Delta$Ms, the instantaneous value of the DAC output at any time during a clock period is important as opposed to DT $\Sigma\Delta$Ms. The ideal pulse waveform of the DAC signal a square pulse, any deviation from this is fed-back to the modulator input, and hence is not noise-shaped by the control loop. Furthermore, CT $\Sigma\Delta$Ms are more sensitive to non-ideal level transitions of the DAC output, such as clock jitter, input–output delay of the DAC and different rise and fall times of the output pulse [10]. One method to alleviate these effects is to use a return-to-zero (RZ) DAC; this was used in the prototype implementation. Furthermore, to reduce $1/f$ noise and dc offset, a chopper stabilization technique was used [13]. A high-performance capacitance to voltage converter (CVC) is critical for capacitive accelerometers. The most important parts of the CVC are: (1) the pick-off amplifier, which should be of low noise and low distortion. Here, a charge amplifier was used for their advantages to sense variations of small differential capacitance; (2) the demodulator, which recovers the original signal from a modulated carrier signal to faithfully reproduce the original signal.

The most common demodulation methods are: synchronous demodulation (lock-in amplification, multiplier demodulation) and diode envelope detection. Spice simulations indicated that there were no commercial components available for synchronous demodulation to recover the original signal from a modulated carrier signal of several MHz with the required accuracy and output amplitude. The diode envelope detection is a good alternative as it balances speed, accuracy and demodulated signal amplitude [14]. The symmetry of the two detection channels is of crucial importance; hence the components selected for the pick-off circuit are all packaged in dual units. The two diodes used for demodulation are Schottky diodes with low forward voltage. A schematic diagram of the demodulation circuit using diode envelope detection is shown in figure 9. An excitation voltage V_{carrier} is applied to the centre of the capacitive half-bridge, which is the proof mass. The stationary electrodes are connected to the input of two charge amplifiers, which are held at virtual ground potential reducing the effects of parasitic capacitances.

The excitation carrier frequency f_{carrier} and the demodulator time constant R_dC_d should be chosen using the following design conditions:

$$f_{\text{carrier}} \gg \frac{1}{2\pi R_f C_F} \gg f_{\text{signal bandwidth}}$$
$$f_{\text{carrier}} \gg \frac{1}{2\pi R_d C_d} \gg f_{\text{signal bandwidth}} \tag{5}$$

where f_{signal} is the sensor bandwidth and the components R_f, R_d, C_F, C_d are defined in figure 9.

The output voltage of the interface circuit can be calculated as

$$V_{\text{out}} = -G_{\text{ina}} V_{\text{carrier}} \frac{(C_{x+} - C_{x-})}{C_F} \cos(\omega_{\text{signal}} t)$$
$$= -G_{\text{ina}} V_{\text{carrier}} \frac{2\Delta C_x}{C_F} \cos(\omega_{\text{signal}} t) \tag{6}$$

where G_{ina} is the gain of the instrumentation amplifier (INA) and ΔC_x is the differential capacitance variation due to accelerations with a frequency ω_{signal}.

The advantage of this CVC is that the circuit is fully differential, so undesired common mode interference is rejected such as switch charge injection and variations in the magnitude of the excitation voltage [3, 14]. It also yields an improved power-supply rejection ratio. The layout of the PCB was designed as symmetrical as possible. Most components of the four-layer PCB are in a SMT package, which lead to low noise and small size.

The first test carried out was to measure the noise floor with a 0 g input signal. The output bitstream was acquired using LabView and a PCI-DIO-32HS data acquisition card [15], triggered by the 125 kHz sampling clock of the quantizer. The acquired bitstream was post-processed with MatLab.

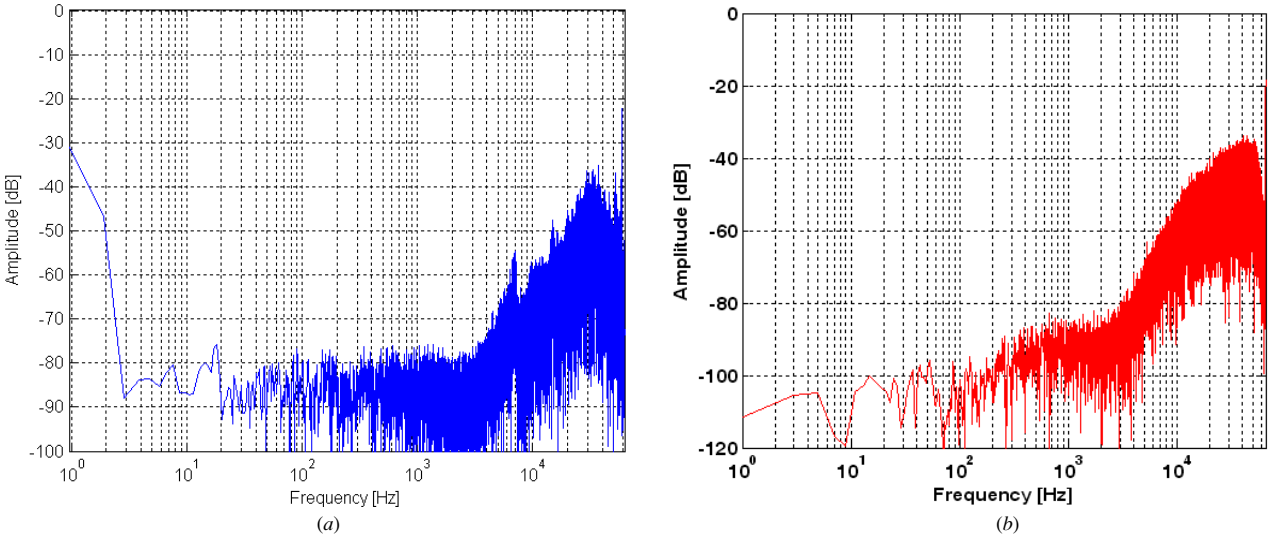

Figure 10. Noise floor of a fifth-order electromechanical $\Sigma\Delta$M: (*a*) measurement and (*b*) simulation.

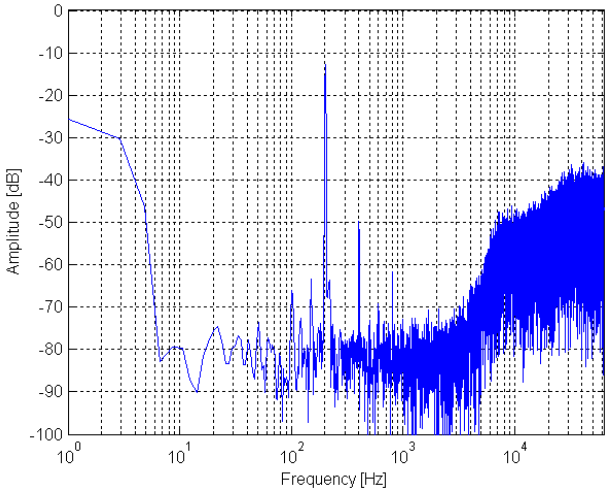

Figure 11. The spectrum of the output bitstream in the fifth-order electromechanical $\Sigma\Delta$M in response to a sinusoidal acceleration with amplitude of -10 dB of the full scale and 200 Hz frequency. Measured by LabView and post-processed by MatLab.

Figure 10(*a*) shows output power spectral density of the bitstream, indicating a noise floor of about -80 dB for the fifth-order electromechanical $\Sigma\Delta$M. This was compared to a simulation which is shown in figure 10(*b*) with the same condition as that of figure 8(*b*), except the input is zero and there is an input-referred electronic noise source of 100 nV Hz$^{-1/2}$ added at the pick-off interface in the simulation model. The noise shaping characteristic is in good agreement to the measured response. However, the noise floor of the measured data is about 5 dB higher; this may be due to electro-magnetic interference noise. As a second test, the prototype was mounted on a shaker table and a sinusoidal acceleration with amplitude of -10 dB of the full scale and 200 Hz frequency was applied to the sensor. Figure 11 shows the spectrum of the output bitstream in a fifth-order electromechanical $\Sigma\Delta$M, post-processed by MatLab. The harmonics in the spectrum of figure 11 are induced by the mechanical shaker and PCB mount, as it was also observed by a reference accelerometer. As expected the noise floor level was not influenced by applying an input acceleration signal.

5. Conclusion

A micromachined accelerometer was designed and fabricated with a mechanical noise floor below 1 μg Hz$^{-1/2}$ and a sensitivity 16 pF g^{-1}. The sensing element was incorporated in a fifth-order $\Sigma\Delta$M force feedback loop which can achieve much better SQNR compared to a second-order loop. Furthermore, the dead zone in a high-order electromechanical $\Sigma\Delta$M is considerably reduced due to the additional electronic filter in the forward path of the control loop. This also alleviates any tonal behaviour. For a prototype implementation a differential capacitive sensing interface was designed with a diode envelope detector for signal demodulation. Measurements indicate that a noise floor of about -80 dB was achieved with a PCB implementation using surface mount technology components. These measurement results agree well with simulations of the fifth-order electromechanical $\Sigma\Delta$M.

References

[1] Seeger J I, Jiang X, Kraft M and Boser B E 2000 Sense finger dynamics in a $\Sigma\Delta$ force-feedback gyroscope *Solid-State Sensor and Actuator Workshop (Hilton Head Island, SC, USA)* pp 296–9

[2] Henrion W *et al* 1990 Wide dynamic range direct digital accelerometer *Solid-State Sensor and Actuator Workshop (Hilton Head Island, SC, USA)* pp 153–7

[3] Lemkin M and Boser B E 1999 A three-axis micromachined accelerometer with a CMOS position-sense interface and digital offset-trim electronics *IEEE J. Solid-State Circuits* **34** 456–68

[4] Petkov V P and Boser B E 2004 A fourth-order $\Sigma\Delta$ interface for micromachined inertial sensors *ISSCC 2004: IEEE Int. Solid-State Circuits Conf.* pp 320–9

[5] Dong Y and Kraft M 2004 Simulation of micromachined inertial sensors with higher-order single loop sigma-delta

modulators *Modeling and Simulation of Microsystems (Boston, USA)* vol 1 pp 414–7
[6] Yazdi N, Ayazi F and Najafi K 1998 Micromachined inertial sensors *Proc. IEEE* **86** 1640–59
[7] Blech J J 1983 On isothermal squeeze films *J. Lubr. Technol.* **105** 615–20
[8] http://www.coventor.com
[9] Norsworthy S R, Schreier R and Temes C 1997 *Delta-Sigma Data Converters, Theory, Design, and Simulation* (NJ: IEEE Press)
[10] Cherry J A and Snelgrove W M 1999 *Continuous-Time Delta-Sigma Modulators for High-Speed A/D Conversion: Theory, Practice and Fundamental Performance Limits* (Dordrecht: Kluwer)
[11] Boser B E and Howe R T 1996 Surface micromachined accelerometers *IEEE J. Solid-State Circuits* **31** 366–75
[12] Hyun D and Fischer G 2002 Limit cycles and pattern noise in single-stage single-bit delta-sigma modulators *IEEE Trans. Circuits Syst. I* **49** 646–56
[13] Enz C C and Temes G C 1996 Circuit techniques for reducing the effects of op-amp imperfections: autozeroing, correlated double sampling, and chopper stabilization *Proc. IEEE* **84** 1584–614
[14] Loetters J C, Olthuis W, Veltink P H and Bergveld P 1999 A sensitive differential capacitance to voltage converter for sensor applications *IEEE Trans. Instrum. Meas.* **48** 89–96
[15] National Instruments, Inc. http://www.ni.com